Andean Geology 50 (1): 75-92. January 2023
doi: 10.5027/andgeoV50n1-3430

Andean Geology
www.andeangeology.cl

Origin of the vanadium-uranium geochemical anomalies in the limestones of the Puyango Formation, La Sota (Ecuador): preliminary results

***John L. Manrique C.[1, 2], José E. Ortiz[2], Antonio Delgado H.[3]**

[1] *Universidad Técnica Particular de Loja, Dpto. Geociencias, Loja, calle Paris, P.O. Box. 11-01-608, Loja, Ecuador. jlmanrique@utpl.edu.ec*

[2] *Universidad Politécnica de Madrid, ETSI Minas y Energía, C/Ríos Rosas 21, P.O. Box 28003, Madrid, España. joseeugenio.ortiz@upm.es*

[3] *Instituto Andaluz de Ciencias de la Tierra (CSIC-UGR), Laboratorio de Biogeoquímica de isótopos estables, Armilla, España. antonio.delgado@csic.es*

** Corresponding author: jlmanrique@utpl.edu.ec*

ABSTRACT. Vanadium (V) and uranium (U) are critical elements for the energy and technology industry. They are characterized by low abundance in the earth crust´s rocks, but can be concentrated and give rise to sedimentary mineral deposits as a result of redox processes during sedimentation and diagenesis. The anomalies of V-U in La Sota, Ecuador, are found in black limestones and black calcareous shales of Cretaceous age. Here we present the results of a geochemical study and a multivariate geostatistical analysis, which enables us to infer four different associations: **1)** disseminated organic matter in the limestones that hold V and Zn, probably in the form of organometallic complexes; **2)** phosphatic minerals and concentrations of U, HREE and Ni, which may be incorporated as trace elements in the phosphates, compatible with sedimentation in an anoxic environment; **3)** Ca in carbonates from a marine environment; and, **4)** litophile elements associated with detritic minerals, such as quartz, plagioclase, feldspar, micas, clays and oxyhydroxides of Fe-Mn-Ti, produced by weathering and erosion. Our findings suggest that V is associated mainly with the organic matter of marine origin in the bituminous limestones, while U is associated with P, thereby indicating the formation of uraniferous phosphates during sedimentation.

Keywords: *Vanadium, Uranium, Geochemistry, Organic matter, Factor analysis.*

RESUMEN. Origen de las anomalías geoquímicas de vanadio-uranio en las calizas de la Formación Puyango, La Sota (Ecuador): resultados preliminares. El vanadio (V) y el uranio (U) son elementos críticos para la industria energética y tecnológica. Se caracterizan por su baja abundancia en las rocas de la corteza terrestre, pero pueden ser concentrados y dar origen a depósitos minerales sedimentarios como resultado de procesos de redox durante la sedimentación y la diagénesis. Las anomalías de V-U en La Sota, Ecuador, se encuentran en calizas negras y lutitas calcáreas negras del Cretácico. En este trabajo se presentan los resultados de un estudio geoquímico y un análisis multivariante, que permite inferir cuatro asociaciones: **1)** materia orgánica diseminada en las calizas que contiene V y Zn, probablemente en forma de complejos organometálicos; **2)** minerales fosfatados y concentraciones de U, HREE y Ni, posiblemente incorporados como elementos traza en los fosfatos, compatibles con sedimentación en un ambiente anóxico; **3)** Ca contenido en carbonatos de ambientes marinos; y, **4)** elementos litófilos asociados a la presencia de minerales detríticos, como cuarzo, plagioclasa, feldespato, micas, arcillas y oxihidróxidos de Fe-Mn-Ti, producidos por meteorización y erosión. Los resultados sugieren que el V está asociado principalmente con la materia orgánica de origen marino diseminada en las calizas bituminosas, mientras que el U está vinculado con el P, lo que indica la formación de fosfatos uraníferos durante la sedimentación.

Palabras clave: *Vanadio, Uranio, Geoquímica, Materia orgánica, Análisis factorial*.

1. Introduction

Vanadium (V) and uranium (U) are two redox-sensitive elements whose sedimentary mineral deposits are mainly linked to ferro-titaniferous sands, bitumen, crude oil and coal in the case of vanadium (Dill, 2010; Pohl, 2011), and to a lesser extent to phosphates and black shales in the uranium case (Cuney and Kyser, 2008; IAEA, 2018). In some areas, U-V deposits hosted in sandstones are formed on oxidation-reduction fronts (roll front) or by precipitation in stratiform reductants (Hou *et al.*, 2007; Cuney, 2009; Dahlkamp, 2009), in which the mobile and soluble U^{6+} is reduced to U^{4+}, and V^{5+}, in turn, is reduced to V^{4+} or V^{3+} (Huang *et al*., 2015).

In unconventional mineral deposits such as black shales, enrichments of V and U can also occur (IAEA, 2018) and are mainly associated with organic matter deposited in restricted marine basins under anoxic conditions, producing organometallic complexes of V such as porphyrins (Gao *et al*., 2013; Huang *et al*., 2015).

Some mineral deposits of U hosted in limestones occur in China, India, Mexico and Greece (Min *et al*., 1997; Nagarajan *et al*., 2011; Tzifas *et al*., 2014; Villarreal *et al*., 2016; IAEA, 2018). A V-U deposit hosted in black limestones is also known in Colombia, named the Berlin deposit (U_3O_8 corp., 2018)[1], which was formed by the chemical reduction of these elements (IAEA, 2009).

In the Alamor-Lancones basin of Cretaceous age in southwestern Ecuador, radiometric anomalies have been associated with the black limestones of the Puyango Formation (Aguilar, 1985), where prospecting studies have recently been initiated (Manrique *et al*., 2018; Manrique, 2019; Manrique-Carreño y Guamán-Jaramillo, 2020). These studies detected geochemical anomalies of V, U and Zn in the La Sota area. Here we aim to identify the origin of these geochemical anomalies of V and U. To this end, we conducted a geochemical study in this area, applying a multivariate statistical analysis to identify the main geochemical associations in samples of bituminous limestones.

2. Geographical and geological setting

The study area is located in the locality of La Sota (Loja province) in the southwestern of Ecuador (Fig. 1). It is characterized by an irregular topography, with abundant vegetation and steep slopes. This area has a dry mega-thermal tropical climate with and average temperature of 24 °C, which, added to the humidity, causes an increase in thermal sensation. The highest rainfall is registered in February, March and April (winter), whereas little or no rainfall occurs during the rest of the year (summer) (G.A.D.M. de Puyango, 2014)[2].

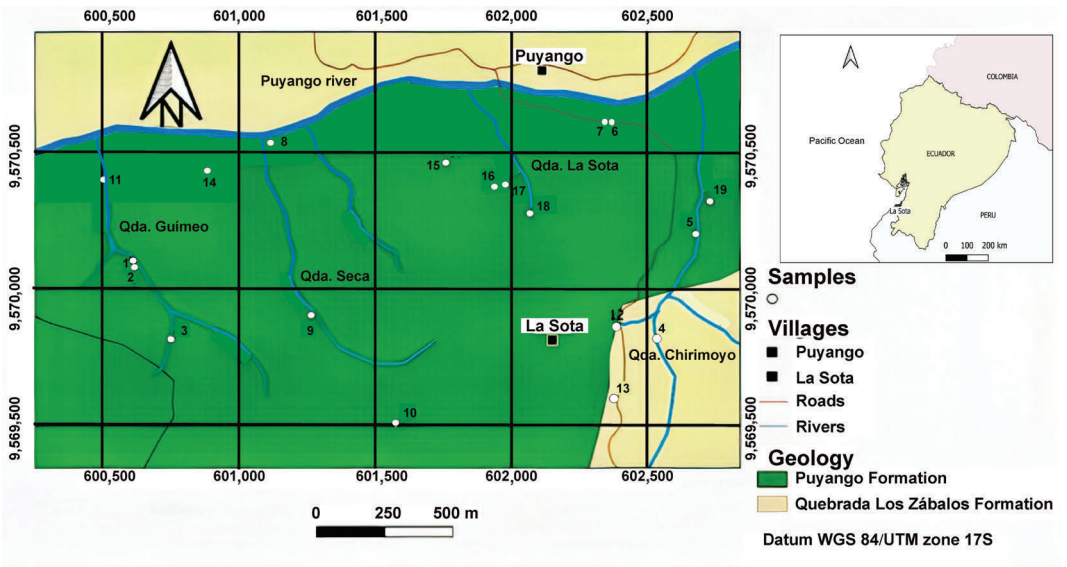

FIG. 1. Geological map of the study area with the location of the sampling sites.

[1] U_3O_8 corporation. 2018. Management's discussion and analysis U_3O_8 corp. Year ended December 31, 2018: 22 p. Toronto.

[2] Gobierno Autónomo Descentralizado del Cantón Puyango (G.A.D.M). 2014. Plan de Desarrollo y Ordenamiento Territorial del Cantón Puyango 2012-2022-Actualización 2014: 332 p. Ciudad.

Two main rock formations of Lower Cretaceous age outcrop in this area, the Quebrada Los Zábalos and Puyango formations (Fig. 2). With an estimated thickness of 400 m, the former consists of siltstones, light gray fine-grained quartz sandstones, fine to medium conglomerates, greenish graywackes embedded with fine-grained gray to medium-grained silicified sandstones, and thin layers of shales (mudstones), deposited in a continental fluvial environment, with development of contemporaneous volcanism (Carrasco, 2018). This formation hosts large fossil trunks and leaf imprints. It overlies pre-Carboniferous sedimentary rocks of El Tigre Formation on a non-conformity and underlies the Puyango Formation (INIGEMM, 2017). The Quebrada Los Zábalos Formation has been attributed an Aptian-Albian age (Jaillard *et al.,* 1999). The Albian-age Puyango Formation (Shoemaker, 1982) consists of sequence of black limestones, turbidites, calcareous shales and calcarenites of *ca*. 300 m thick, deposited in an open platform as a result of marine transgression. These rocks are strongly deformed and present calcite veinlets. The presence of fossil remains is very common, including mainly ammonites, bivalves and small corals. It is capped by the Chaquino Formation of the Zapotillo Group with an angular unconformity (Jaillard *et al*., 1999).

Preliminary studies by Celi (2011) found high concentrations of U in the areas of La Sota and Puyango, linked to apatite. Furthermore, significant amounts of U bearing minerals, such as fluorapatite and uranosphatite, and V minerals, such as sherwoodite and ronneburgite have been identified in the area within bituminous black limestones of the Puyango Formation, which are probably related to geochemical anomalies of V, U and Zn (Manrique *et al.*, 2018; Manrique, 2019).

3. Materials and methods

3.1. Sampling and sample preparation

A total of 19 rock samples were taken from outcrops in which stratigraphic sections were recognized (Fig. 3): 16 samples are from limestones from the Puyango Formation sections, whereas three (4, 12, 13) are siliciclastic rocks from the Quebrada Los Zábalos Formation (Table 1). We chose to sample these stratigraphic sections as they were the best outcrops in the area. In addition, promising exploration results were obtained in a previous research with the identification of U, V, Zn anomalies in this area (Manrique *et al*., 2018). Samples of *ca*. 2 kg were recovered after removing the surficial 20 cm to avoid the presence of weathered and/or eroded material. The sampled stratigraphic sequences are shown in Fig. 3. Sections 1, 7 and 8 belong to the Puyango Formation and they are composed mainly of intercalations of black limestone and calcareous shales. The stratigraphic sequence of the Quebrada Los Zábalos Formation, section number 4 in figure 3, consists mainly of siliciclastic

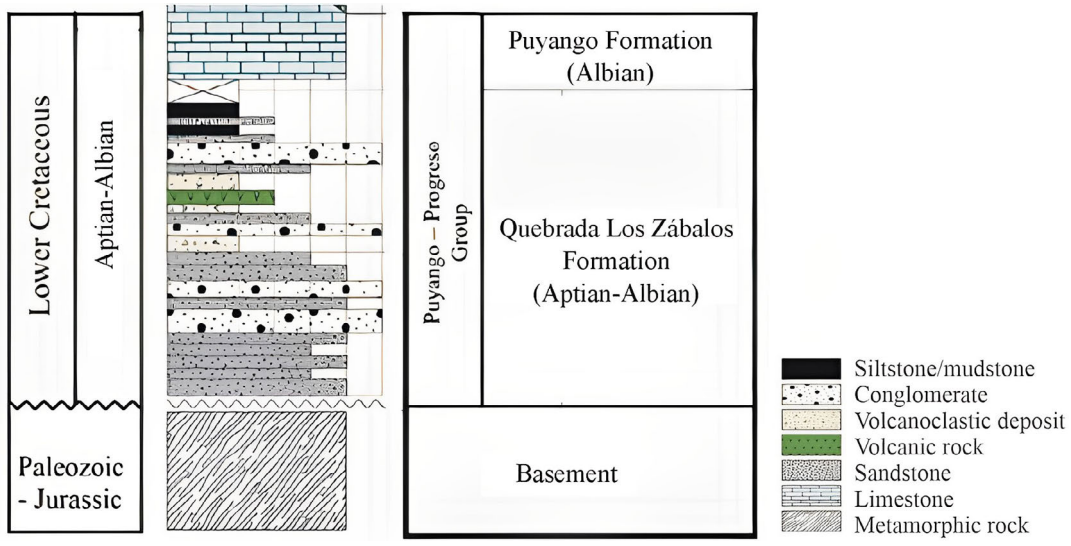

FIG. 2. Stratigraphic positions of Puyango and Quebrada Los Zábalos formations (modified from Carrasco, 2018).

TABLE 1. CHARACTERISTICS OF THE SAMPLES.

Sample	Formation	Lithology
1	Puyango	Grey limestone
2	Puyango	Grey limestone
3	Puyango	Grey limestone
4	Qda. Los Zábalos	Brown sandstone
5	Puyango	Grey limestone
6	Puyango	Black calcareous shale
7	Puyango	Grey calcareous marl
8	Puyango	Black limestone
9	Puyango	Black limestone
10	Puyango	Grey limestone
11	Qda. Los Zábalos	Brown sandstone
12	Qda. Los Zábalos	Brown sandstone
13	Puyango	Grey limestone
14	Puyango	Black limestone
15	Puyango	Black limestone
16	Puyango	Black limestone
17	Puyango	Grey limestone
18	Puyango	Black limestone
19	Puyango	Grey limestone

sandstones. Samples were placed in sealed bags to avoid external contamination and labeled accordingly. All samples were georeferenced. Two sub-samples were separated from the samples: one for multi-element inorganic chemical analysis, and another for total organic carbon (TOC) determination.

The samples were dried at 105 ºC for 24 h at the Laboratory of Geology and Mining (Geosciences Department of the Universidad Técnica Particular de Loja). Then comminution was done to obtain <5 cm fragments. The fragmented samples were crushed in a jaw crusher and <3 mm fractions were separated and adequately quartered in a cracker. About 200 g of the representative samples were loaded to the grinder for 3 min to produce a sample of 200 g. Then the sample was pulverized during 3 min in a vibratory disc mill of agata, to produce a particle size of approximately 0.5 to 20 microns after which it was removed in a sealed case and its corresponding label. All devices were thoroughly cleaned with ethanol between each sample preparation.

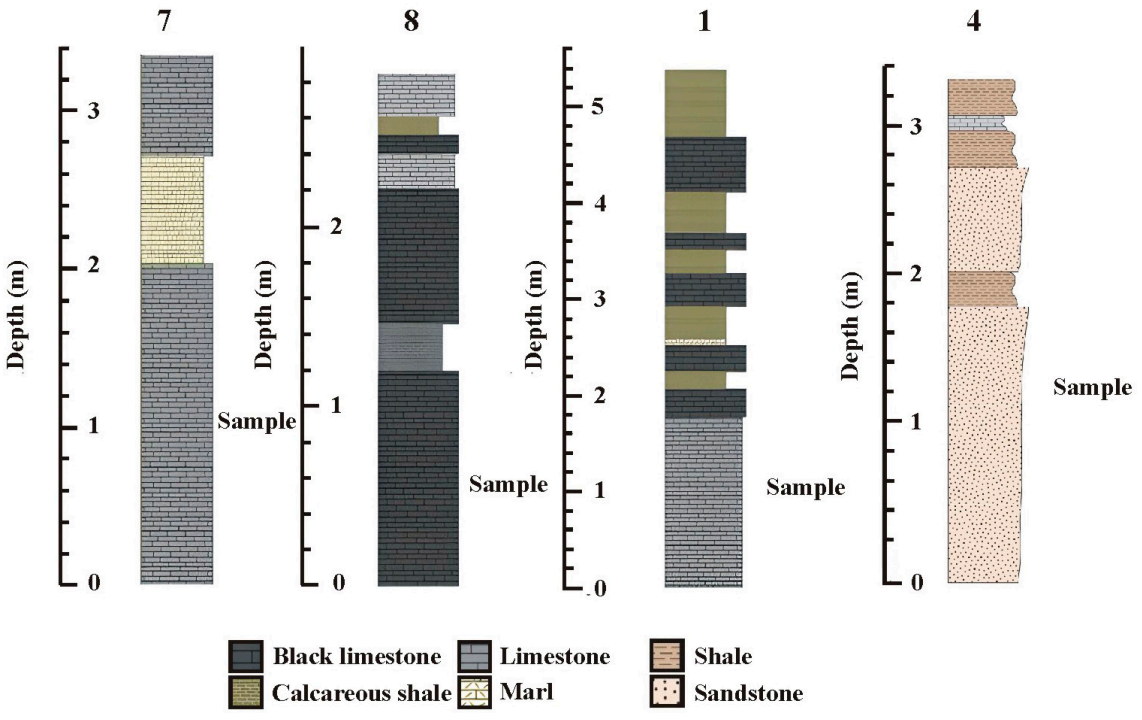

FIG. 3. Stratigraphy of the sampling area. The number above each stratigraphic column corresponds to the sampling point shown in figure 1.

3.2. Multi-element inorganic chemical analysis

Samples were analyzed by an ISO 17025 (Lab 266) and NELAP (Lab E87979) accredited laboratory: Activation Laboratories Ltd. (Actlabs, Ontario, Canada). For QA/QC purposes, five blanks (analytical and method), five duplicates, and ten analyses of standard reference materials (internal standards, OREAS45EA and SdAR-M2) were inserted in the sequences of samples to provide a measure of background noise, accuracy, and precision. Samples were analyzed by inductively coupled plasma-mass spectrometry (ICP-MS) using the 4LITHORES (11+) Major Elements Fusion, ICP(WRA)/Trace Elements Fusion ICP/MS(WRA4B2) package offered by Actlabs. The analytical precision was <2% and the accuracy better than 5 at 95% confidence level. Detection limit for major elements was 0.01%, with the exception of TiO_2 and MnO (0.001%), whereas detection limit for trace elements varied between 0.01 and 5 mg/kg depending on the element.

3.3. Total Organic Carbon (TOC) analysis

Another sub-set of the same 19 samples were used for TOC analysis in the Laboratorio de Biogeoquímica de Isótopos Estables (Instituto Andaluz de Ciencias de la Tierra). These samples (1 g) were homogenized with a mortar and pestle. TOC was determined using a Shimadzu TOC analyzer.

3.4. Statistical analysis

For the statistical study, 37 elements determined in the studied samples were considered (light and heavy rare earth elements were grouped within LREE and HREE, respectively), since in all cases the data were above the detection limits, and also the total organic carbon (TOC). The multi-element matrix was compiled to build a database that was studied using Statistica 10.0 software.

This multi-element matrix was used to perform a cluster analysis to establish geochemical groups of samples, mainly limestones, with analogous behavior. We also performed a cluster analysis to examine the elements with similar behavior. Ward´s algorithm and Euclidean distance were used.

A factor analysis was also performed to reduce dimensionality, which makes it possible to simplify the explanation of a set of observations. The data cloud is explained in terms of major axes derived from the covariance matrix by extracting the eigenvectors and subsequently deriving a matrix with factor loadings, which explain the common variability of these original variables (element concentrations in our case).

4. Results

4.1. Raw data and chemical composition of samples

The concentration of the major elements in the analyzed samples is shown in figure 4. The results confirmed that the limestones belonging to the Puyango Formation display a low content of MgO. The detrital component was significant, as evidenced by the concentration of SiO_2 ranging between 10 and 20 wt%. Also of note was the presence of organic matter (TOC) with an average content of 6.25 wt%. Minor components were Al_2O_3 and Fe_2O_3.

The chemical composition of the three samples belonging to the Quebrada Los Zábalos. Formation (4, 11 and 12) clearly differs from those of the Puyango Formation (Fig. 4) as they showed high SiO_2 concentrations, followed by Al_2O_3 and Fe_2O_3. In contrast, the concentration of CaO was <5 wt%, which agrees with its siliciclastic nature. In addition, the concentration of trace elements also showed differences between samples from the Puyango and Quebrada Los Zábalos formations (Fig. 5).

4.2. Chemical anomalies

The background values (median), threshold (median+standard deviation), sub-anomalies (median+2 standard deviation) and anomalies (median+ 3 standard deviation) of the studied samples were calculated for all elements (Table 2) following the methodology used by Howarth (1983). Light and heavy rare earth elements were grouped within LREE and HREE, respectively.

Significant anomalous values were obtained for MgO (1.73 wt.%), P_2O_5 (2.47 wt%) and TOC (>25.03 wt%). All of them are associated with the Cretaceous bituminous limestones of the Puyango Formation. Regarding the trace elements, anomalous values were obtained for elements of economic interest: V (>3,569 mg/kg), HREE (>147 mg/kg), Zr (>26 mg/kg), Co (>0 mg/kg), Ni (>17 mg/kg), Cu (>30 mg/kg), Zn (>2,615 mg/kg) and U (>195 mg/kg). Of these, the redox-sensitive elements to be highlighted are V, U and Zn. The spatial distribution of these anomalies is shown in the geochemical maps in figures 6 and 7.

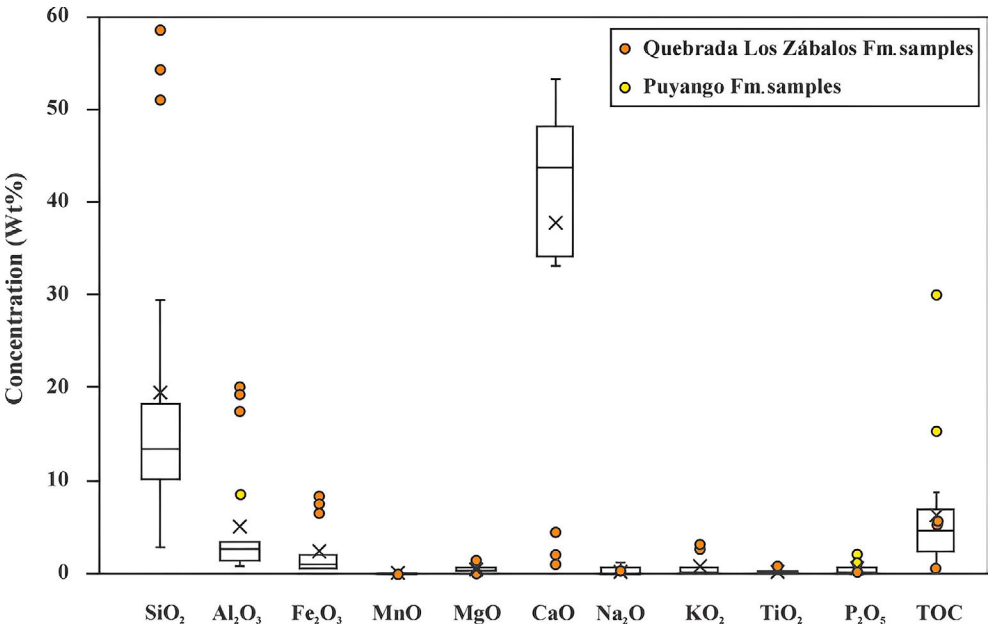

FIG. 4. Box-plot diagram for major elements of the samples. Limestone samples from the Puyango Formation. Samples from the Los Zábalos Formation are plotted separately. X represents the median.

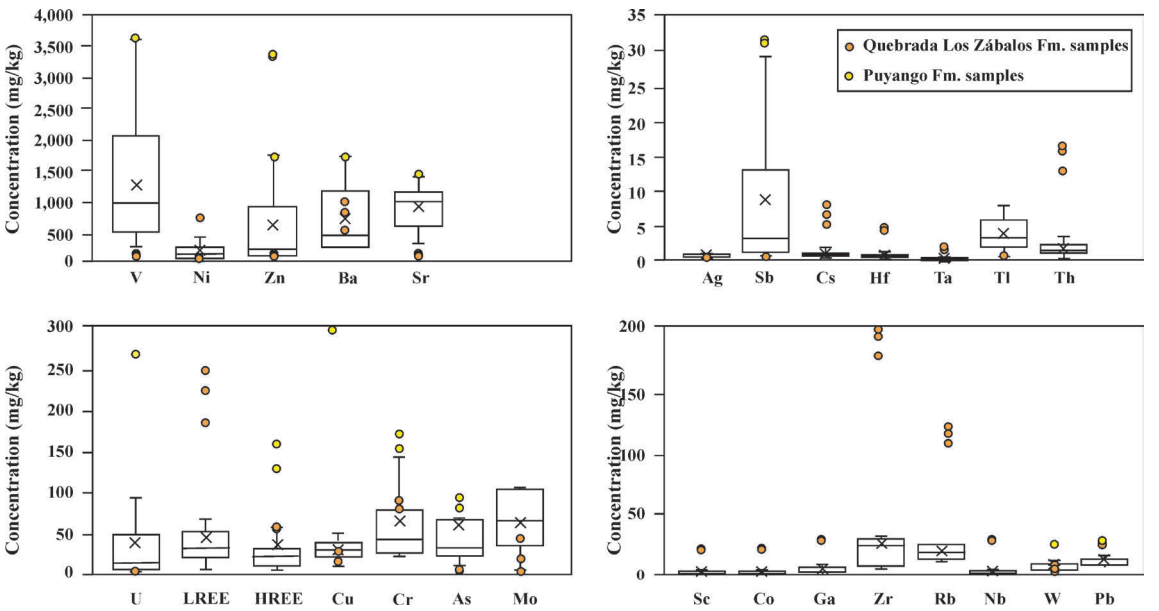

FIG. 5. Box-plot diagrams for trace element contents in limestone samples from the Puyango Formation. Samples from Quebrada Los Zábalos Formation are plotted separately. X represents the median.

TABLE 2. GEOCHEMICAL BACKGROUND, THRESHOLD, SUB-ANOMALIES AND ANOMALIES DETERMINED FOR THE ANALYZED ELEMENTS IN THE STUDIED SAMPLES.

	Background	Threshold	Sub-anomaly	Anomaly
SiO_2 (wt%)	13.28	29.86	46.45	-
Al_2O_3 (wt%)	2.70	9.07	15.44	-
Fe_2O_3(T) (wt%)	0.98	3.82	6.66	-
MnO (wt%)	0.03	0.05	0.08	-
MgO (wt%)	0.55	0.94	1.34	1.73
CaO (wt%)	43.65	-	-	-
Na_2O (wt%)	0.14	0.42	0.70	0.98
K_2O (wt%)	0.41	1.30	2.19	-
TiO_2 (wt%)	0.14	0.44	0.73	-
P_2O_5 (wt%)	0.26	1.00	1.73	2.47
TOC (wt%)	4.66	11.45	18.24	25.03
Sc (mg/kg)	3	9	15	-
V (mg/kg)	627	1,608	2,589	3,569
Ba (mg/kg)	568	1,061	1,553	-
Sr (mg/kg)	682	1,097	-	-
Zr (mg/kg)	29	95	160	226
Cr (mg/kg)	60	107	155	-
Co (mg/kg)	1	7	14	20
Ni (mg/kg)	80	259	438	617
Cu (mg/kg)	30	130	230	330
Zn (mg/kg)	170	985	1,800	2,615
Ga (mg/kg)	4	12	20	-
As (mg/kg)	9	35	60	86
Rb (mg/kg)	14	54	95	-
Nb (mg/kg)	2	10	18	-
Mo (mg/kg)	52	88	124	-
Ag (mg/kg)	0.5	0.7	1.0	1.2
Sb (mg/kg)	2.6	13.6	24.5	-
Cs (mg/kg)	0.9	3.4	5.9	8.4
Hf (mg/kg)	0.7	2.2	3.7	-
Ta (mg/kg)	0.1	0.6	1.2	1.7
W (mg/kg)	2.0	7.8	13.6	19.4
Tl (mg/kg)	3.0	5.4	7.8	-
Pb (mg/kg)	6.0	13.7	21.5	-
Th (mg/kg)	1.5	6.8	12.0	-
U (mg/kg)	11.1	72.3	133.5	194.8
Σ LREE (mg/kg)	35.2	113.7	192.1	-
Σ HREE (mg/kg)	22.9	64.4	105.8	147.3

Background (median), Threshold (median +1*standard deviation), Sub-anomaly (median +2*standard deviation) and, Anomaly (median +3*standard deviation). - represents does not reach the category.

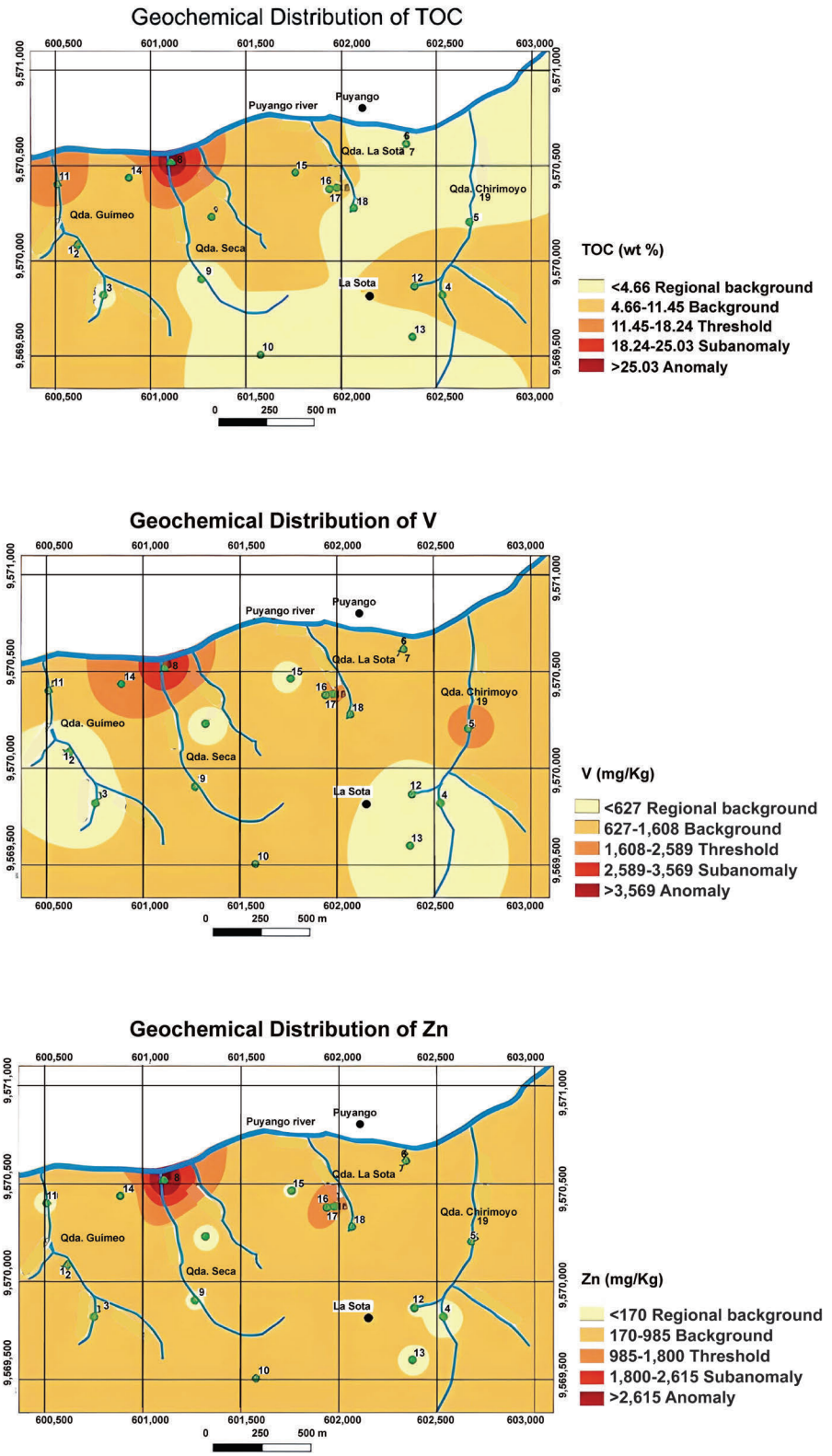

FIG. 6. Geochemical distributions of TOC, V and Zn.

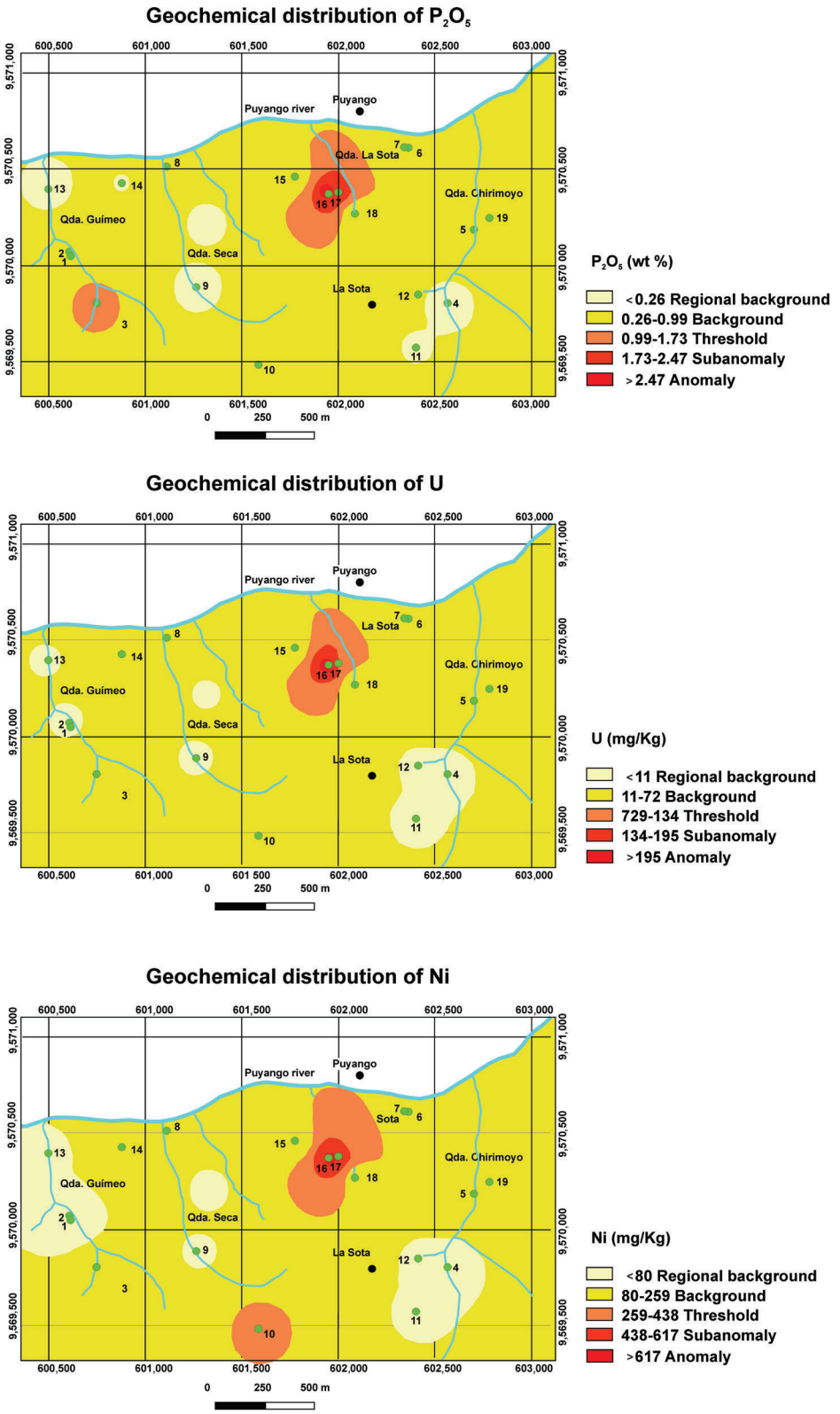

FIG. 7. Geochemical distributions of P_2O_5, U and, Ni.

4.3. Multivariate statistical analysis

The results of the cluster and factor analysis are presented in figures 8, 9 and 10 and tables 3 and 4.

5. Discussion

Based on the geochemical maps (Figs. 6 and 7) the following spatial associations of anomalies and sub-anomalies were obtained: **1)** TOC, V and Zn in samples 8, 18, 17, 15 and 5; and **2)** P, U and Ni in samples 17 and 18. These results were corroborated by cluster analysis (Fig. 8) and factor analysis (Fig. 10).

5.1. Multivariate statistical analysis

5.1.1. Cluster analysis of the studied samples

The dendrogram (Fig. 8) for the samples shows two clusters, the first one comprising 5 samples (cluster A) which consist of limestones, and the second one 14 (B), which could be divided into sub-clusters (B1 and B2).

Cluster A includes the samples with the highest concentration of V (Table 3) and shows a V enrichment that is approximately 10 to 24 times higher than that of the clarke (150 mg/kg, Dill, 2010), thereby evidencing the anomaly in this area. Samples 8 and 17 of this cluster show the highest Zn contents and both represent limestones of the Puyango Formation.

Cluster B includes a subgroup (B1) with samples that have the highest concentrations of SiO_2 and Al_2O_3 (4, 11, 12). These samples corresponded to the siliciclastic rocks of the Quebrada Los Zábalos Formation, and they show the lowest concentrations of V, Zn and U (Table 3), all below the background values calculated in the present study (Table 2). Although they belong to limestones of the Puyango Formation, samples 2 and 9 were included in this subgroup due to their low concentrations of V, Zn and U.

In the other subgroup (B2), the samples show V, Zn and U concentrations (Table 3) falling between the background categories to sub anomalies according to the geostatistical analysis of the present study (Table 2). All these samples corresponded to bituminous limestones of the Puyango Formation.

5.1.2. Cluster analysis of the studied samples chemical composition

The cluster analysis conducted for the chemical elements determined in the studied samples identified two main groups (Fig. 9). In addition, the correlation matrix was calculated for all the elements considered. The correlation coefficients obtained (Table 2 Supplementary information) together with the cluster analysis groups make possible to identify those chemical elements with a probable common origin.

Cluster A contains two subgroups: A1, including Sr and Ba, which may be associated with carbonate,

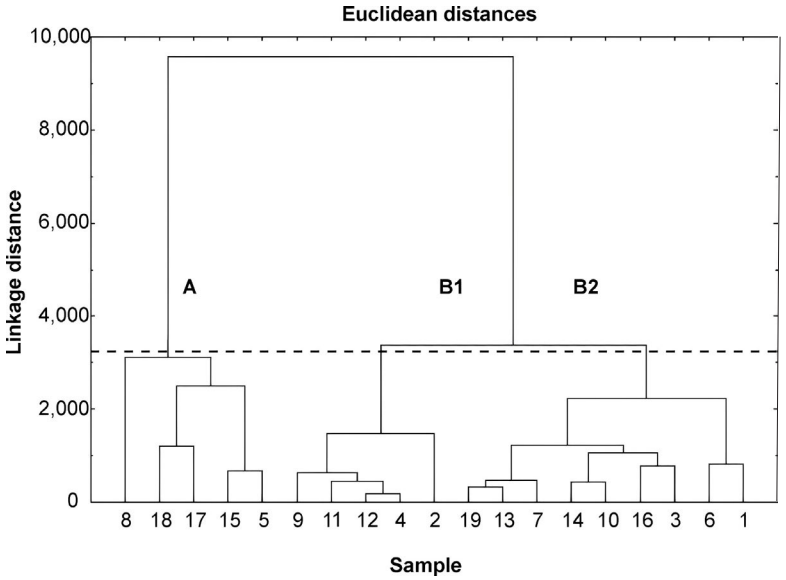

FIG. 8. Dendrogram obtained (Ward method) for cluster analysis of the studied samples.

TABLE 3. MEAN OF U, V AND ZN CONCENTRATIONS IN SUB GROUPS CLUSTERS OF THE STUDIED SAMPLES.

Mean/sub groups	U (mg/kg)	V (mg/kg)	Zn (mg/kg)
A	90.1	2,353	1,366
B1	5.4	162	100
B2	14.9	644	333

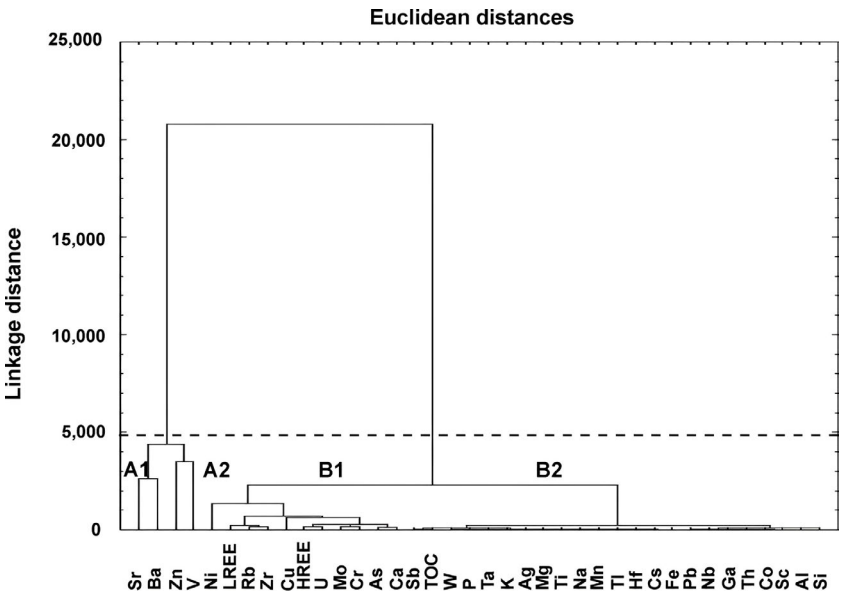

FIG. 9. Dendrogram obtained (Ward method) for cluster analysis of chemical elements.

where Ba and Sr can replace Ca in calcite of the limestones included in the Puyango Formation (Lan *et al.,* 1988; Van *et al.,* 2003; Tardy, 1975), and A2, including Zn and V, which may be related to the potential presence of organometallic complexes in the bituminous black limestones of the same Formation (Breit and Wanty, 1991; Huang *et al.,* 2015; Gao *et al.,* 2013). V, Zn, Mo and TOC showed high correlation coefficients (Table 2 Supplementary information), consistent with that shown in figure 6, where a spatial coincidence of the V-Zn-TOC anomalies is observed. This finding may be explained by the fact that these elements are bound and/or absorbed in organic matter (Breit and Wanty, 1991). In this regard, V can form organometallic complexes such as porphyrins, which are organic molecules of marine origin (Gao *et al.,* 2013). In addition, Zn and Mo can also form organometallic complexes (Huang *et al.,* 2015).

Cluster B (Fig. 9) also has two subgroups: B1, including Ni, LREE, Rb, Zr, Cu, HREE, U, Mo, Cr, As and Ca, which are mostly pathfinders of sedimentary U deposits, mainly Mo, Ni, Cu and As (Cuney and Kyser, 2008; Cuney, 2009; Dahlkamp, 2009), and B2, grouping Sb, TOC, W, P, Ta, K, Ag, Mg, Ti, Na, Mn, Tl, Hf, Cs, Fe, Pb, Nb, Ga, Th, Co, Sc, Al and Si, most of which are lithophile elements and reflect the presence of detrital mineral in the analyzed samples (Bhathia and Crook, 1986; Kidder *et al.,* 2003), namely Si, Al, K, Fe, Ti, Sc, Zr, Co, Ga, Rb, Nb, Cs, Hf, Ta, Pb, Th, and LREE. These elements are possibly hosted in silicates and aluminosilicates, such as quartz, feldspars, plagioclase, micas (biotite, muscovite), clays and oxyhydroxides of Fe, (Misra, 2012) and zircon ($ZrSiO_4$).

Subgroup B2 also includes other elements of chalcophile character, namely Sb, Ag, Pb and Co, which could be part of sulfurs or sulfosalts associated with organic matter (Misra, 2012) or be present as ionic substitutions of Fe, Mn or Ti in ferrous silicates or ferric oxyhydroxides (Pohl, 2011).

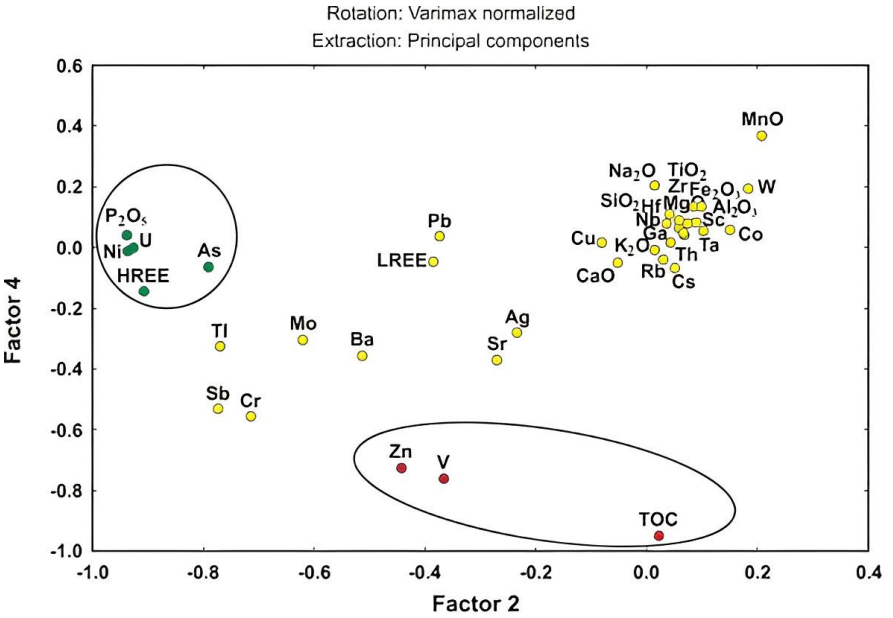

FIG. 10. Factor 2 *versus* Factor 4 scatter diagram of principal component analysis (PCA) using the rotation method with varimax normalized. Zn-V-TOC association is indicated by the red dots included in the ellipse and the HREE-U-P_2O_5-Ni-As association by the green dots enclosed by the circle.

5.1.3. Geochemical associations based on factorial analysis

On the basis of the discriminant analysis, four factors explaining more than 90% of the original variance were deduced for the samples. The main results of the factor analysis are shown in table 4 (after varimax rotation). The variables show sufficient communality (the proportion of variance of such a variable shared with the others and accounted for by common factors) to validate the results. Therefore, the interpretation of the factor loadings is as follows:

Factor 1 groups mainly lithophile elements (Si, Al, Fe, K, Ti, Sc, Zr, Co, Ga, Rb, Nb, Cs, Hf, Ta, Pb, Th, LREE) hosted in detrital minerals. In this factor, Ca shows a negative correlation with the other elements of Factor 1, which is interpreted as an inverse relationship between the presence of limestones, composed mainly by $CaCO_3$, and detrital minerals (quartz, plagioclase, feldspar, micas, clays, oxyhydroxides of Fe-Mn-Ti).

Factor 2 mainly groups P, U, HREE and Ni, together with Cr, As, Sb and Tl. This grouping may be explained by the presence of phosphate minerals, such as apatite, that can host these trace elements in their crystal lattices (Saw, 1952; McArthur and Walsh, 1984).

Factor 3 shows an association between Cu, Ag and Na. The chalcophile nature of the first two suggests that limestone may contain small amounts of sulfides (*e.g.,* chalcopyrite, chalcocite) and therefore future research should analyze S. Some sedimentary Cu deposits are formed in sediments deposited in shallow marine, deltaic and saline lacustrine environments by brines that move through the sediments and whose metal content is derived from buried sedimentary and volcanic rocks (Tourtelot and Viene, 1976; Cox *et al.,* 2003), which may explain the association of Na with Cu and Ag here.

Factor 4 consists mainly of TOC, V and Zn, which is compatible with the detected V-Zn anomaly associated with the organic matter disseminated in the bituminous limestones of the Puyango Formation, as observed in figure 6.

The Principal Component Analysis (PCA) using the rotation method with varimax normalized (Fig. 10) shows the association between Zn, V and TOC in the lower part of the diagram. However, these elements are somewhat distanced on the horizontal axis (Factor 2), which may imply that V and Zn could occur in organic and inorganic forms. Several elements also grouped in the upper right section of the plot. These mostly corresponded to lithophile elements that form minerals of detrital origin and carbonates.

TABLE 4. FACTOR LOADINGS (VARIMAX NORMALIZED).

	Factor 1	Factor 2	Factor 3	Factor 4
SiO_2	0.961	0.041	0.083	0.113
Al_2O_3	0.964	0.088	0.216	0.085
Fe_2O_3	0.882	0.097	0.420	0.135
MnO	0.524	0.207	0.561	0.371
MgO	0.632	0.065	0.606	0.051
CaO	-0.972	-0.052	-0.171	-0.047
Na_2O	0.487	0.012	0.784	0.205
K_2O	0.996	0.013	0.010	-0.007
TiO_2	0.983	0.073	0.125	0.082
P_2O_5	-0.097	-0.939	-0.071	0.043
TOC	-0.068	0.021	-0.123	-0.947
Sc	0.934	0.084	0.262	0.135
V	-0.260	-0.366	-0.058	-0.758
Ba	0.153	-0.513	-0.081	-0.353
Sr	-0.631	-0.271	-0.323	-0.368
Zr	0.973	0.057	0.022	0.091
Cr	0.350	-0.715	-0.076	-0.554
Co	0.961	0.150	0.066	0.060
Ni	-0.145	-0.937	0.106	-0.010
Cu	-0.113	-0.082	0.965	0.019
Zn	-0.126	-0.443	0.291	-0.723
Ga	0.983	0.057	0.132	0.067
As	-0.106	-0.791	0.540	-0.060
Rb	0.996	0.029	-0.010	-0.038
Nb	0.992	0.067	-0.036	0.041
Mo	-0.245	-0.620	0.106	-0.301
Ag	0.236	-0.234	0.865	-0.278
Sb	-0.122	-0.774	0.274	-0.530
Cs	0.987	0.050	-0.012	-0.064
Hf	0.985	0.034	0.028	0.081
Ta	0.987	0.102	-0.024	0.055
W	-0.026	0.181	0.004	0.194
Tl	-0.321	-0.769	-0.028	-0.323
Pb	0.839	-0.374	0.317	0.037
Th	0.994	0.042	-0.023	0.019
U	-0.097	-0.926	-0.094	0.000
LREE	0.912	-0.386	-0.024	-0.043
HREE	0.349	-0.908	-0.014	-0.142
Expl. Variance	55.1	24.0	7.5	4.8

Thus, according to the factor analysis, the following four geochemical associations can be inferred: **1)** disseminated organic matter (TOC) in the limestones in which V and Zn are hosted, probably forming organometallic complexes; **2)** phosphatic minerals that contain high concentrations of U, HREE and Ni as trace elements, both associations probably formed during sedimentation in an anoxic environment (Shields and Stille 2001; Kidder *et al.,* 2003); **3)** Ca which forms mainly calcite that composes the limestones of the Puyango Formation (INIGEMM, 2013) and; **4)** Litophile elements contained in detritic minerals, such as quartz, plagioclase, feldspar, micas, clays and oxyhydroxides of Fe-Mn-Ti, caused by the clastic contribution within the sedimentary basin and, in this study, associated mainly with the calcareous shales of the Puyango Formation, and on the other hand, corresponding to the samples of fluvial origin belonging to the Quebrada Los Zábalos Formation.

5.2. Vanadium in the black limestone of Puyango Formation

Based on the multivariate statistical analysis presented above, V was probably associated mainly with organic matter of marine origin, disseminated in the bituminous black limestones. In these environments V has the ability to form organometallic complexes such as porphyrins. Porphyrins are organic compounds formed by a pyrrolic ring and with a V atom bound at their center, similar to the chlorophyll molecule (Breit and Wanty, 1991; Gao *et al.,* 2013), in which V replaces the Mg during diagenesis, under suboxic to anoxic conditions (Huang *et al*., 2015; Gao *et al*., 2013).

Similarly, V may have accumulated independently of organic matter, as there are samples with high concentrations of V but low TOC values. This finding agrees with previous reports of vanadate minerals as sherwoodite and ronneburgite observed in limestones of the Puyango Formation (Manrique *et al*., 2018; Manrique, 2019; Manrique-Carreño and Guamán-Jaramillo, 2020). These minerals may have been formed by the weathering of previously mineralized rocks hosting V^{3+} and V^{4+} bearing minerals (Gao *et al*., 2013), producing vanadates with V^{5+} under oxidizing conditions (Gao *et al*., 2013; Bowell, 2019). Another possibility is that V is present as V^{3+} in aluminosilicates (samples 4 and 13), which show sub-anomalous values of Sc, thereby indicating the presence of phyllosilicate-type minerals. V is also associated with Zn and TOC, as evidenced by the cluster and factor analysis (Figs. 9 and 10). This observation suggests that V-C_{org} and Zn-C_{org} organometallic complexes should have been formed (Scott *et al*., 2017).

6. Uranium in the black limestones of the Puyango Formation

The association between P_2O_5, U and HREE (Figs. 7 and 10), observed in the bituminous limestones of the Puyango Formation, could be explained by the formation of apatite ($Ca_5(PO_4)_3(Cl,F,OH)$, in whose crystal lattice ionic substitutions of U^{4+}, Ce^{4+} and REE^{4+} can occur (Shields and Stille 2001; Kidder *et al*., 2003). In addition, the U-P_2O_5 association suggests the formation of U-bearing phosphates during limestone sedimentation (Hughes and Rakovan, 2015), this is corroborated by previous studies in the La Sota area, in which apatite and uranosphatite have been found in the bituminous limestones from the Puyango Formation showing U geochemical anomalies (Manrique *et al*., 2018; Manrique, 2019, Manrique-Carreño and Guamán-Jaramillo, 2020).

Deposits of uraniferous phosphates have been reported around the world (Dahlkamp, 2009; IAEA, 2018), but they are considered by the IAEA (2018) as unconventional deposits because the grades are low (100 mg/kg on median). In the La Sota area, we identified limestone layers enriched in uraniferous phosphates and found that U is not directly related to V in the mineralized zone (Manrique, 2019).

7. Conclusions

In the La Sota area the geochemical V anomaly (>3,569 mg/kg) is accompanied by high Zn (>2,615 mg/kg) and TOC (>25.03 wt%) contents, and spatially related to the bituminous black limestones of the Puyango Formation. Whereas, U shows anomalies exceeding 195 mg/kg together with high concentrations of P_2O_5 (>2.47 wt%), and Ni (>617 mg/kg).

The statistical analysis of the studied bituminous limestone samples from the Puyango Formation, identified four main geochemical association corresponding to: **1)** V-Zn-TOC, **2)** P_2O_5-U-HREE-Ni, **3)** Ca and **4)** Si-Al-Fe_K-Ti-Sc-Zr-Co- Ga-Rb-Nb-Cs, Hf-Ta-Pb-Th-LREE. The first one suggests that V and Zn may be absorbed in organic matter, in particular V,

forming organometallic complexes *e.g.,* porphyrins. The second association is probably associated with phosphate minerals, such as apatite, hosted in the black limestones of the Puyango Formation. Ca represents mainly the calcite content of the limestones, and the last association is reflecting the detrital minerals content in the sedimentary rocks of the study area.

Acknowledgments

This project was funded by the Universidad Técnica Particular de Loja (UTPL), Ecuador-Innovation Project: "Preliminary study for the extraction of vanadium from sedimentary mines and the prospection of lithium as sources of raw material for batteries", project code: PROY_INNOV_2019_2605. We also thank Fundación Carolina for the grant of one of us (JLM) during 2020, Spain. Students D. Calderon and F. Angamarca are thanked for their work in the field and in the laboratory. We thank Prof. A. Martin Testi and Prof. W. Vivallo for their valuable and helpful comments on the manuscript.

References

Aguiar, E. 1985. Exploración de uranio en el Ecuador: Período 1980-1985. Technical report (Unpublished). Escuela Politécnica del Ejército: 34 p. Quito.

Bhatia, R.; Crook, W. 1986. Trace element characteristics of graywackes and tectonic setting discrimination of sedimentary basins. Contributions to Mineralogy and Petrology 92 (2): 181-193. doi: https://doi.org/10.1007/bf00375292.

Bowell, R,. 2019. An introduction to vanadium, Chemistry, Occurrences and Applications. Nova Sciences Publishers: 350 p. New York.

Breit, G.N.; Wanty, R.B. 1991. Vanadium accumulation in carbonaceous rocks: A review of geochemical controls during deposition and diagenesis. Chemical Geology 91: 83-97. doi: https://doi.org/10.1016/0009-2541(91)90083-4

Carrasco, H. 2018. Análisis litoestratigráfico y de procedencia de los depósitos sedimentarios cretácicos de la cuenca Alamor-Lancones. Trabajo de Titulación previo a la obtención del título de Ingeniero Geólogo (Inédito). Escuela Politécnica Nacional: 129 p. Quito.

Celi, D. 2011. Estudio del procesamiento de un mineral de apatitas uraníferas en la zona del Puyango. Trabajo de Titulación previo a la obtención del título de Ingeniería Química (Inédito). Escuela Politécnica Nacional: 262 p. Quito.

Cox, D.; Lindsey, D.; Singer, D.; Moring, B.; Diggles, M. 2003. Sediment-Hosted Copper Deposits of the World: Deposits Models and Database. United States Geological Survey. Open-File Report 03-107: 53 p. Denver.

Cuney, M. 2009. The extreme diversity of uranium deposits. Mineralium Deposita 44: 3-9.

Cuney, M.; Kyser, K. 2008. Recent and not so recent developments in uranium deposits and implications for exploration. Mineralogical Association of Canada. Short Course Series 39: 501 p. Canada.

Dahlkamp, F.J. 2009. Uranium deposits of the world, Part I Typology of uranium deposits: Asia Springer-Verlag: 494 p. Berlin Heidelberg.

Dill, H. 2010. The "chessboard" classification scheme of mineral deposits: Mineralogy and geology from aluminum to zirconium. Earth Science Reviews 100 (1-4): 1-420. doi: https://doi.org/10.1016/j.earscirev.2009.10.011.

Gao, Y.; Shen, B.; Liu, J. 2013. Distribution of nickel and vanadium in Venezuelan crude oil. Petroleum Sciences and Technolology 31 (5): 509-515. doi: https://doi.org/10.1080/10916466.2011.576363

Huang, J.; Huang, F.; Evans, L.; Glasauer, S. 2015. Vanadium: Global (bio)geochemistry. Chemical Geology 417: 68-89. doi: https://doi.org/10.1016/j.chemgeo.2015.09.019

Hughes, J.; Rakovan, J. 2015. Structurally Robust, Chemically Diverse: Apatite and Apatite Supergroup Minerals. Elements 11 (3): 165-170. doi: https://doi.org/10.2113/gselements.11.3.165

IAEA. 2009. World Distribution of Uranium Deposits (UDEPO) with Uranium Deposit Classification. International Agency Energy Atomic. IAEA-TECDOC-1629: 128 p. Vienna.

IAEA. 2018. Geological classification of uranium deposits and description of selected examples. International Agency Energy Atomic. IAEA-TECDOC-1842: 428 p. Vienna.

INIGEMM. 2013. Hoja Geológica Puyango, escala 1:50.000. Instituto Nacional de Investigación Geológico Minero Metalúrgico, 1 mapa escala 1:50.000. Quito.

INIGEMM. 2017. Hoja Geológica Puyango. Hoja 21, M VI-F. Instituto Nacional de Investigación Geológico Minero Metalúrgico, 1 mapa escala 1:100.000. Quito.

Jaillard, E.; Laubacher, G.; Bengtson, P.; Dhondt, A.; Bulot, L. 1999. Stratigraphy and evolution of the Cretaceous forearc Celica-Lancones basin of southwestern Ecuador. Journal of South American Earth Sciences 12 (1): 51-68. doi: https://doi.org/10.1016/S0895-9811(99)00006-1

Kidder, L.; Krishnaswamy, R.; Mapes, H. 2003. Elemental mobility in phosphatic shales during concretion

growth and implications for provenance analysis. Chemical Geology 198 (3-4): 335-353. doi: https://doi.org/10.1016/s0009-2541(03)00036-6

Lan, C.; Yang, B.; Peng, S. 1988. Environment for forming major coal-seams of Permian coal-bearing series in Huainan coalfield. Journal of Coal Science and Engineering 1: 11-22.

Manrique, J. 2019. Geochemical anomalies of vanadium and uranium in black limestones in Puyango, Ecuador, case of study. *In* An introduction to vanadium, Chemistry, Occurrences and Applications (Bowell, R.; editor). Nova Sciences Publishers: 119-139. New York.

Manrique, J.; Guamán, G.; Guartán, J. 2018. Geochemical prospecting study of the vanadium-uranium mineralization of Puyango, Ecuador. *In* IAEA International Symposium on Uranium Raw Material for the Nuclear Fuel Cycle: Exploration, Mining, Production, Supply and Demand, Economics and Environmental Issues, Book of Abstracts and Extended Abstracts: 260-262. Vienna.

Manrique-Carreño, J.; Guamán-Jaramillo, G. 2020. Estudio de prospección geoquímica en sedimentos de las microcuencas Chirimoyo y Guineo, Ecuador Boletín de Geología: 42 (1): 39-55. doi: https://doi.org/10.18273/revbol.v42n1-2020002

McArthur, M.; Walsh, N. 1984. Rare-earth geochemistry of phosphorites. Chemical Geology 47 (3-4): 191-220. doi: https://doi.org/10.1016/0009-2541(84)90126-8

Min, M.; Zheng, D.; Shen, B.; Wen, G.; Wang, X.; Gandhi, S. 1997. Genesis of the Sanbaqi deposit: a paleokarst-hosted uranium deposit in China. Mineralium Deposita 32: 505-519. doi: https://doi.org/10.1007/s001260050118

Misra, K. 2012. Introduction to Geochemistry. Principles and Applications. Wiley-Blackwell: 456 p. Oxford.

Nagarajan, R.; Madhavaraju, J.; Armstrong, J.; Nagendra, R. 2011. Geochemistry of Neoproterozoic limestones of the Shahabad Formation, Bhima Basin, Karnataka, southern India. Geosciences Journal 15 (1): 9-25. doi: https://doi.org/10.1007/s12303-011-0005-0.

Pohl, W. 2011. Economic Geology: Principles and Practice. Metals, Minerals, Coal and Hydrocarbons-Introduction to Formation and Sustainable Exploitation of Mineral Deposits. Wiley-Blackwell: 699 p. Oxford.

Saw, D. 1952. The geochemistry of thallium. Geochimica et Cosmochimica Acta 2: 118-154.

Scott, C.; Slack, J.; Kelley, K. 2017. The hyper-enrichment of V and Zn in black shales of the Late Devonian-Early Mississippian Bakken Formation (USA). Chemical Geology 452: 24-33. doi: https://doi.org/10.1016/j.chemgeo.2017.01.026

Shields, G.; Stille, P. 2001. Diagenetic constraints on the use of cerium anomalies as palaeoseawater redox proxies: an isotopic and REE study of Cambrian phosphorites. Chemical Geology 175 (1-2): 29-48. doi: https://doi.org/10.1016/s0009-2541(00)00362-4

Shoemaker, R. 1982. Fossil leaves from de Lower Cretaceous Ciano Formation southwestern Ecuador. Palaeontograhica Abteilung B 180 (4-6): 120-132.

Tourtelot, E.B.; Vine, J.D. 1976. Copper Deposits in Sedimentary and Volcanogenic Rocks. United States Geological Survey, Professional Paper 907-c: 44 p. Washington.

Tzifas, I.; Godelitsas, A.; Magganas, A.; Androulakaki, E.; Eleftherioucd, G.; Mertzimekisa, T.; Perrakie, M. 2014. Uranium-bearing phosphatized limestones of NW Greece. Journal of Geochemical Exploration 143: 62-73. doi: https://doi.org/10.1016/j.gexplo.2014.03.009

Van, B.; Reyss, J.; Bonte, P.; Schmidt, S. 2003. Sr/Ba in barite: a proxy of barite preservation in marine sediments? Marine Geology 199 (3-4): 205-220. doi: https://doi.org/10.1016/S0025-3227(03)00220-2

Villarreal-Fuentes, J.; Levresse, G.; Nieto-Samaniego, A.; Alexandre, P.; Corona-Esquivel, R. 2016. Geochemistry and geochronology of the Sierra de Gomez Limestone-hosted U deposit, Chihuahua: Implications for distribution of Rio Grande rift mineral deposits in northern Mexico. Ore Geology Reviews 76: 19-34. doi: https://doi.org/10.1016/j.oregeorev.2016.01.004

Manuscript received: September 15, 2021; revised/accepted: June 6, 2022; available online: September 30, 2022.

SUPPLEMENTARY INFORMATION

TABLE 1. STATISTICAL PARAMETERS OF THE SAMPLES FROM THE PUYANGO FORMATION.

	Minimum	Maximum	Mean	Median	Standard deviation
SiO_2 (wt%)	2.89	29.35	12.87	12.18	5.97
Al_2O_3 (wt%)	0.87	8.41	2.54	2.27	1.79
Fe_2O_3 (T) (wt%)	0.36	6.45	1.31	0.86	1.46
MnO (wt%)	0.01	0.08	0.03	0.02	0.02
MgO (wt%)	0.13	1.44	0.52	0.45	0.28
CaO (wt%)	33.00	53.16	44.30	44.70	5.29
Na_2O (wt%)	0.03	1.09	0.20	0.11	0.27
K_2O (wt%)	0.07	0.76	0.38	0.38	0.16
TiO_2 (wt%)	0.04	0.28	0.13	0.12	0.07
P_2O_5 (wt%)	0.07	2.80	0.62	0.29	0.79
TOC (wt%)	0.25	29.74	6.55	4.59	7.28
Sc (mg/kg)	1	10	4	3	3
V (mg/kg)	83	3,607	1,119	895	999
Ba (mg/kg)	253	1,744	709	446	531
Sr (mg/kg)	316	1,399	854	985	340
Zr (mg/kg)	10	51	29	27	12
Cr (mg/kg)	20	170	61	40	51
Co (mg/kg)	1	4	1	1	1
Ni (mg/kg)	20	740	182	120	188
Cu (mg/kg)	10	460	60	30	108
Zn (mg/kg)	30	3,340	620	235	870
Ga (mg/kg)	1	8	3	3	2
As (mg/kg)	5	88	23	11	27
Rb (mg/kg)	3	30	14	13	7
Nb (mg/kg)	1	4	2	2	1
Mo (mg/kg)	2	100	59	61	36
Ag (mg/kg)	0.5	1.4	0.6	0.5	0.3
Sb (mg/kg)	0.6	32.6	8.6	3.0	11.6
Cs (mg/kg)	0.5	1.8	0.9	0.7	0.4
Hf (mg/kg)	0.2	1.2	0.7	0.6	0.3
Ta (mg/kg)	0.1	0.3	0.1	0.1	0.1
W (mg/kg)	1	25	4	1	6
Tl (mg/kg)	0.5	7.9	3.8	3.2	2.3
Pb (mg/kg)	5	19	8	5	5
Th (mg/kg)	0.3	3.3	1.5	1.4	0.7
U (mg/kg)	3.8	266.0	37.4	12.6	65.7
Σ LREE (mg/kg)	6.64	162.58	46.42	31.50	45.06
Σ HREE (mg/kg)	5.29	157.82	35.41	21.72	44.27

TABLE 2. CORRELATION MATRIX OF THE SAMPLES FROM THE PUYANGO FORMATION.

	SiO_2	Al_2O_3	Fe_2O_3	MnO	MgO	CaO	Na_2O	K_2O	TiO_2	P_2O_5	Sc	V	Ba	Sr	Zr	Cr	Co	Ni	Cu	Zn	Ga	Ge	As	Rb	Nb	Mo	Ag	Sb	Cs	Hf	Ta	W	Tl	Pb	Th	U	LREE
Al_2O_3	0.96	-	-	-	-	-	-	-	-	-	-	-	-	-	-	-	-	-	-	-	-	-	-	-	-	-	-	-	-	-	-	-	-	-	-	-	-
Fe_2O_3	0.91	0.97	-	-	-	-	-	-	-	-	-	-	-	-	-	-	-	-	-	-	-	-	-	-	-	-	-	-	-	-	-	-	-	-	-	-	-
MnO	0.56	0.57	0.66	-	-	-	-	-	-	-	-	-	-	-	-	-	-	-	-	-	-	-	-	-	-	-	-	-	-	-	-	-	-	-	-	-	-
MgO	0.56	0.66	0.72	0.77	-	-	-	-	-	-	-	-	-	-	-	-	-	-	-	-	-	-	-	-	-	-	-	-	-	-	-	-	-	-	-	-	-
CaO	-0.99	-0.99	-0.95	-0.57	-0.62	-	-	-	-	-	-	-	-	-	-	-	-	-	-	-	-	-	-	-	-	-	-	-	-	-	-	-	-	-	-	-	-
Na_2O	0.55	0.67	0.77	0.70	0.81	-0.62	-	-	-	-	-	-	-	-	-	-	-	-	-	-	-	-	-	-	-	-	-	-	-	-	-	-	-	-	-	-	-
K_2O	0.96	0.97	0.91	0.43	0.54	-0.98	0.51	-	-	-	-	-	-	-	-	-	-	-	-	-	-	-	-	-	-	-	-	-	-	-	-	-	-	-	-	-	-
TiO_2	0.98	0.99	0.95	0.55	0.62	-0.99	0.61	0.99	-	-	-	-	-	-	-	-	-	-	-	-	-	-	-	-	-	-	-	-	-	-	-	-	-	-	-	-	-
P_2O_5	-0.17	-0.20	-0.23	-0.28	-0.14	0.19	-0.06	-0.13	-0.19	-	-	-	-	-	-	-	-	-	-	-	-	-	-	-	-	-	-	-	-	-	-	-	-	-	-	-	-
Sc	0.96	0.98	0.97	0.63	0.66	-0.98	0.68	0.95	0.98	-0.21	-	-	-	-	-	-	-	-	-	-	-	-	-	-	-	-	-	-	-	-	-	-	-	-	-	-	-
V	-0.35	-0.41	-0.42	-0.40	-0.26	0.33	-0.41	-0.32	-0.39	0.25	-0.42	-	-	-	-	-	-	-	-	-	-	-	-	-	-	-	-	-	-	-	-	-	-	-	-	-	-
Ba	0.05	0.07	-0.02	-0.30	-0.03	-0.06	0.09	0.15	0.08	0.64	0.02	0.21	-	-	-	-	-	-	-	-	-	-	-	-	-	-	-	-	-	-	-	-	-	-	-	-	-
Sr	-0.73	-0.76	-0.78	-0.63	-0.51	0.73	-0.62	-0.68	-0.75	0.31	-0.79	0.67	0.09	-	-	-	-	-	-	-	-	-	-	-	-	-	-	-	-	-	-	-	-	-	-	-	-
Zr	0.98	0.96	0.91	0.50	0.53	-0.97	0.52	0.98	0.98	-0.17	0.94	-0.38	0.09	-0.72	-	-	-	-	-	-	-	-	-	-	-	-	-	-	-	-	-	-	-	-	-	-	-
Cr	0.26	0.21	0.14	-0.15	0.10	-0.27	-0.05	0.33	0.24	0.57	0.19	0.64	0.54	0.15	0.26	-	-	-	-	-	-	-	-	-	-	-	-	-	-	-	-	-	-	-	-	-	-
Co	0.94	0.97	0.92	0.40	0.50	-0.96	0.55	0.97	0.97	-0.24	0.94	-0.41	0.06	-0.72	0.96	0.17	-	-	-	-	-	-	-	-	-	-	-	-	-	-	-	-	-	-	-	-	-
Ni	-0.22	-0.25	-0.21	-0.17	-0.07	0.22	-0.07	-0.22	-0.25	0.82	-0.23	0.45	0.30	0.35	-0.25	0.61	-0.32	-	-	-	-	-	-	-	-	-	-	-	-	-	-	-	-	-	-	-	-
Cu	-0.06	0.06	0.26	0.45	0.48	-0.02	0.67	-0.12	-0.03	-0.01	0.09	0.04	-0.16	-0.15	-0.12	-0.08	-0.06	0.23	-	-	-	-	-	-	-	-	-	-	-	-	-	-	-	-	-	-	-
Zn	-0.22	-0.20	-0.17	-0.22	0.03	0.16	-0.04	-0.18	-0.21	0.38	-0.20	0.71	0.34	0.28	-0.24	0.64	-0.24	0.53	0.32	-	-	-	-	-	-	-	-	-	-	-	-	-	-	-	-	-	-
Ga	0.96	0.99	0.96	0.50	0.60	-0.98	0.60	0.99	0.99	-0.18	0.98	-0.38	0.09	-0.73	0.97	0.24	0.98	-0.24	-0.01	-0.20	-	-	-	-	-	-	-	-	-	-	-	-	-	-	-	-	-
Ge	0.95	0.97	0.91	0.44	0.53	-0.96	0.50	0.99	0.98	-0.23	0.94	-0.40	0.06	-0.71	0.98	0.21	0.98	-0.32	-0.15	-0.25	0.98	-	-	-	-	-	-	-	-	-	-	-	-	-	-	-	-
As	-0.15	-0.11	-0.01	0.04	0.16	0.11	0.29	-0.15	-0.14	0.71	-0.09	0.34	0.36	0.16	-0.18	0.53	-0.22	0.80	0.61	0.51	-0.13	-0.26	-	-	-	-	-	-	-	-	-	-	-	-	-	-	-
Rb	0.96	0.97	0.90	0.40	0.52	-0.97	0.48	-	0.98	-0.15	0.94	-0.29	0.13	-0.66	0.97	0.33	0.98	-0.23	-0.13	-0.17	0.99	0.99	-0.17	-	-	-	-	-	-	-	-	-	-	-	-	-	-
Nb	0.95	0.97	0.90	0.41	0.52	-0.96	0.48	0.99	0.98	-0.18	0.94	-0.36	0.08	-0.68	0.98	0.27	0.98	-0.26	-0.16	-0.23	0.98	0.99	-0.21	-	-	-	-	-	-	-	-	-	-	-	-	-	-
Mo	-0.28	-0.36	-0.30	-0.13	-0.21	0.28	-0.25	-0.32	-0.35	0.44	-0.32	0.78	0.08	0.55	-0.33	0.57	-0.42	0.74	0.25	0.55	-0.35	-0.42	0.61	-0.32	-0.37	-	-	-	-	-	-	-	-	-	-	-	-
Ag	0.30	0.39	0.52	0.39	0.56	-0.37	0.72	0.29	0.33	0.10	0.40	0.14	0.19	-0.31	0.27	0.35	0.29	0.22	0.81	0.46	0.34	0.23	0.66	0.28	0.23	0.23	-	-	-	-	-	-	-	-	-	-	-
Sb	-0.22	-0.21	-0.19	-0.26	0.00	0.18	0.00	-0.17	-0.22	0.70	-0.22	0.70	0.51	0.38	-0.24	0.78	-0.27	0.77	0.33	0.84	-0.21	-0.28	0.82	-0.17	-0.24	0.67	0.53	-	-	-	-	-	-	-	-	-	-
Cs	0.94	0.96	0.90	0.39	0.54	-0.96	0.48	0.99	0.97	-0.17	0.94	-0.29	0.13	-0.67	0.95	0.33	0.97	-0.24	-0.13	-0.15	0.98	0.98	-0.18	0.99	0.99	-0.33	0.26	-0.17	-	-	-	-	-	-	-	-	-
Hf	0.98	0.97	0.92	0.50	0.56	-0.98	0.53	0.99	0.99	-0.16	0.95	-0.37	0.10	-0.72	-	0.28	0.96	-0.23	-0.11	-0.22	0.98	0.98	-0.16	0.98	0.98	-0.32	0.28	-0.22	0.97	-	-	-	-	-	-	-	-
Ta	0.95	0.97	0.90	0.44	0.53	-0.96	0.48	0.99	0.98	-0.20	0.94	-0.38	0.07	-0.70	0.97	0.24	0.97	-0.30	-0.15	-0.26	0.98	0.99	-0.22	0.99	-	-0.39	0.23	-0.26	0.98	0.98	-	-	-	-	-	-	-
W	0.01	0.02	-0.03	0.03	-0.02	0.02	0.23	-0.02	0.02	-0.04	-0.03	-0.32	0.38	-0.15	0.05	-0.32	0.04	-0.25	-0.11	-0.26	-0.02	0.00	-0.22	-0.05	-0.04	-0.36	-0.14	-0.26	-0.06	0.03	-0.04	-	-	-	-	-	-
Tl	-0.42	-0.46	-0.44	-0.40	-0.27	0.41	-0.32	-0.39	-0.44	0.64	-0.43	0.74	0.31	0.63	-0.43	0.63	-0.50	0.84	0.10	0.58	-0.43	-0.49	0.66	-0.38	-0.43	0.87	0.13	0.78	-0.39	-0.41	-0.47	-0.27	-	-	-	-	-
Pb	0.85	0.89	0.88	0.39	0.57	-0.88	0.66	0.88	0.87	0.18	0.86	-0.22	0.26	-0.59	0.85	0.46	0.86	0.12	0.20	0.02	0.89	0.83	0.29	0.87	0.85	-0.10	0.58	0.16	0.85	0.86	0.84	-0.13	-0.14	-	-	-	-
Th	0.95	0.97	0.90	0.41	0.53	-0.97	0.49	0.99	0.98	-0.16	0.94	-0.34	0.11	-0.68	0.97	0.29	0.98	-0.24	-0.14	-0.21	0.99	0.99	-0.18	-	-	-0.35	0.25	-0.21	0.99	0.98	0.99	-0.04	-0.41	0.87	-	-	-
U	-0.18	-0.21	-0.23	-0.31	-0.11	0.19	-0.11	-0.15	-0.21	0.91	-0.22	0.34	0.43	0.37	-0.19	0.58	-0.24	0.90	0.01	0.49	-0.18	-0.22	0.63	-0.16	-0.18	0.51	0.05	0.70	-0.17	-0.18	-0.22	-0.20	0.69	0.16	-0.16	-	-
LREE	0.88	0.87	0.80	0.27	0.46	-0.88	0.45	0.93	0.89	0.21	0.84	-0.16	0.34	-0.54	0.88	0.57	0.87	0.11	-0.12	0.01	0.90	0.87	0.12	0.92	0.91	-0.12	0.33	0.13	0.92	0.90	0.90	-0.09	-0.11	0.93	0.92	0.20	-
HREE	0.32	0.29	0.23	-0.09	0.16	-0.32	0.16	0.37	0.30	0.81	0.27	0.28	0.59	0.00	0.32	0.85	0.25	0.73	-0.01	0.44	0.32	0.27	0.65	0.36	0.33	0.39	0.34	0.71	0.35	0.34	0.30	-0.18	0.52	0.62	0.35	0.79	0.68